

Design of a line-start synchronous reluctance motor

*Original*

Design of a line-start synchronous reluctance motor / Gamba, Matteo; Pellegrino, GIAN - MARIO LUIGI; Vagati, Alfredo; Villata, Franco. - STAMPA. - (2013), pp. 648-655. ( 2013 International Electric Machines & Drives Conference Chicago, USA Maggio 2013) [10.1109/IEMDC.2013.6556163].

*Availability:*

This version is available at: 11583/2518606 since: 2016-01-13T13:10:05Z

*Publisher:*

IEEE

*Published*

DOI:10.1109/IEMDC.2013.6556163

*Terms of use:*

This article is made available under terms and conditions as specified in the corresponding bibliographic description in the repository

*Publisher copyright*

IEEE postprint/Author's Accepted Manuscript

©2013 IEEE. Personal use of this material is permitted. Permission from IEEE must be obtained for all other uses, in any current or future media, including reprinting/republishing this material for advertising or promotional purposes, creating new collecting works, for resale or lists, or reuse of any copyrighted component of this work in other works.

(Article begins on next page)

# Design of a Line-Start Synchronous Reluctance motor

M. Gamba, G. Pellegrino, *Senior Member, IEEE*, A. Vagati, *Fellow, IEEE*, and F. Villata

**Abstract**—The design of line-start Synchronous Reluctance machines is proposed, based on the state of the art of motors designed for closed loop, vector control. The guidelines for overcoming the dilemma between synchronization capability and steady state performance are given, with examples of good and bad design choices. The proposed solutions compared via finite element analysis with a competitor induction motor in terms of efficiency and power factor. The finite element calculations are finally validated via experiments on a laboratory prototype.

**Index Terms** – Synchronous Reluctance Machine, Induction Motor, Line Start Motor, High Efficiency Motor, Fixed Speed Drives.

## I. INTRODUCTION

Line-start synchronous motors are adopted in alternative to line-supplied Induction Motors (IM) due to their better efficiency [1-3]. All the cited examples refer to permanent magnet (PM) line start motors, and this has been true since the introduction of rare-earth PMs back in the 1970s. The volatility of rare earth materials prices over the last couple of years has led to reconsider the Synchronous Reluctance (SyR) machine as a viable alternative to PM line-start motors for constant speed applications where line start motors are applicable. Line-Start SyR (LSSyR) machines were studied and adopted in the '60s and the '70s [4-5]. At that time, such machines were voltage supplied by means of variable frequency inverters to obtain exact speeds, that were not possible at the time with the induction motor counterparts [6]. Lately, the diffusion of vector controlled IM drives with a precise speed control, on the one hand, and of PM based line start machines with a higher torque density, on the other hand, have led to abandon LSSyR motors.

In retrospect, being the literature about LSSyR rather aged, all the improvements of SyR motor design emerged between now and the '70s have never been tested in line-start applications. The research upon SyR motors for vector-controlled drives has produced up to date multi-barrier rotors [7], having better saliencies than the ones adopted for LSSyR in the literature, and disclosing a potential for a higher torque and a better power factor at synchronous speed.

This work proposes the design of a LSSyR motor for pumps application, based on a SyR rotor with four flux barriers filled with aluminum completely and short-circuited at both ends of the stack to from the rotor cage. The design of the rotor laminations is based on the state of the art of SyR machines design, with some little modifications that show to improve

the starting capability of the machine. The design guidelines for obtaining the best compromise between the pull-in and pull-out torque values are given. The pull-in torque represents the synchronization capability intended as the maximum load that can be put into step. The pull-out torque represents the performance at synchronous speed, meaning the maximum load applicable at synchronism. Pull-in and pull-out capabilities are in contrast with each other, to a certain extent, and a compromise is given.

A lumped parameters model of the motor is presented, and simulated in the time domain to investigate the pull-in transients. From the same model the steady state torque is expressed analytically, as a function of the slip speed between the voltage vector, defining the synchronous speed, and the rotor. The lumped parameters approach gives precious hints but it is not very accurate in terms of evaluating the pull-in torque and the inertia that can be actually put into step. Finite Element Analysis (FEA) simulations of the transient with motion type are then used, and the pull into step curve of the different motors under test is evaluated as a function of the total inertia to be synchronized. All tested LSSyR solutions are compared at steady state with the an IM competitor having the same frame and the same stator laminations and windings. Last, a prototype SyR machine, equipped with a cage made with welded copper bars partially filling the saliencies, is tested for checking the validity of the transient with motion FEA.

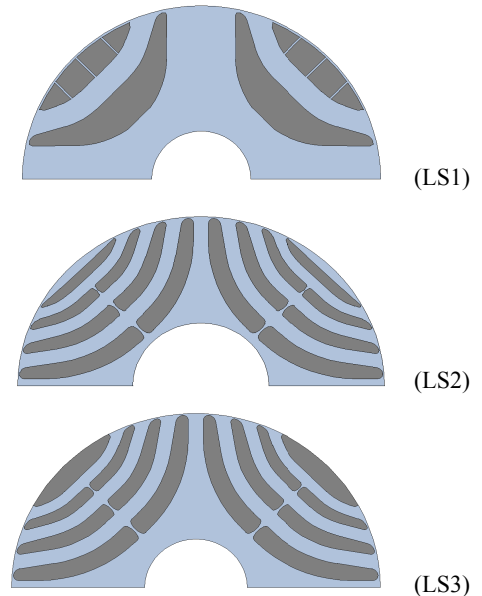


Figure 1. Line Start SyR motors rotors under investigation: LS1 is a synduction motor-like solution [4]. LS2 is a state of the art SyR rotor filled with aluminum (dark grey areas). LS3 is the proposed LSSyR solution.

## II. MODELING OF THE LSSyR MACHINE

The dynamic model of the LSSyR machine accounts for the concurrent presence of rotor saliency, as in a SyR machine, and a short circuited rotor cage, as in an Induction Motor [1]. The  $dq$  reference frame, synchronous to the rotor, is defined in Fig. 2. The rotor speed, in electrical radians, is  $\omega_r$ . The voltage vector, also in Fig. 2, is imposed by the AC mains that define the angular frequency  $\omega$  and the synchronous speed  $\omega/p$ , where  $p$  is the number of pole pairs. In the rotor frame, the voltage slips at  $\omega - \omega_r$  and the slip  $s$  is defined according to:

$$s = \frac{\omega - \omega_r}{\omega} \quad (1)$$

The phase angle  $\delta$  of the voltage vector is also defined in Fig. 2.

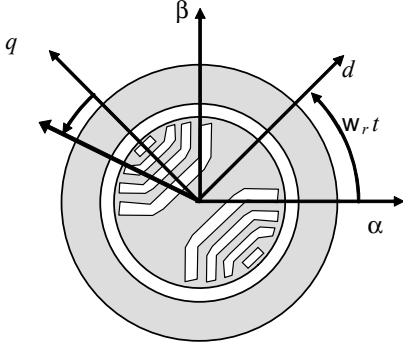


Figure 2. Definition of the stator and rotor synchronous reference frames. Definition of the synchronous speed  $\omega$ .

The rotor cage is not housed in usual rotor slots, all the same and regularly displaced along the airgap periphery, as it would be in an asynchronous motor. On the contrary, the cage conductors here are aluminum bars that fill the saliencies of the SyR rotor completely, as in the examples of Fig. 1.

### A. Dynamic model

With reference to the circuitual model reported in Fig 3 for the  $d$  and  $q$  axes, the electrical equations of the motor are:

$$\bar{v}_s = R_s \bar{i}_s + \frac{d\bar{\lambda}_s}{dt} + j\omega_r \bar{\lambda}_s \quad (2)$$

$$0 = \begin{bmatrix} R_{rd} & 0 \\ 0 & R_{rq} \end{bmatrix} \cdot \bar{i}_r + \frac{d\bar{\lambda}_r}{dt} \quad (3)$$

$$0 = R_{fe} \bar{i}_{fe} + \frac{d\bar{\lambda}_m}{dt} \quad (4)$$

The subscript  $s$  stands for “stator” variables, whilst the subscript  $r$  stands for “rotor”. The non isotropic shape of the cage bars is reflected into the rotor parameters of the model, and then the rotor resistances are different for the  $d$  and  $q$  axes in (3). The magnetic model is:

$$\bar{\lambda}_s = L_{\sigma s} \bar{i}_s + \begin{bmatrix} L_{md} & 0 \\ 0 & L_{mq} \end{bmatrix} \cdot \bar{i}_m \quad (5)$$

$$\bar{\lambda}_r = \begin{bmatrix} L_{\sigma rd} & 0 \\ 0 & L_{\sigma rq} \end{bmatrix} \cdot \bar{i}_r + \begin{bmatrix} L_{md} & 0 \\ 0 & L_{mq} \end{bmatrix} \cdot \bar{i}_m \quad (6)$$

$$\bar{i}_m = \bar{i}_s + \bar{i}_r \quad (7)$$

Where  $L_{md}$  and  $L_{mq}$  are the magnetizing inductances.  $L_{\sigma s}$  and  $L_{\sigma r}$  are the stator and rotor leakage inductances, respectively. As for the rotor resistances, also the rotor leakage inductances are not equal in  $d$  and  $q$  in (6). Basically, all the parameters of the circuit related to the rotor reflect the rotor anisotropy.

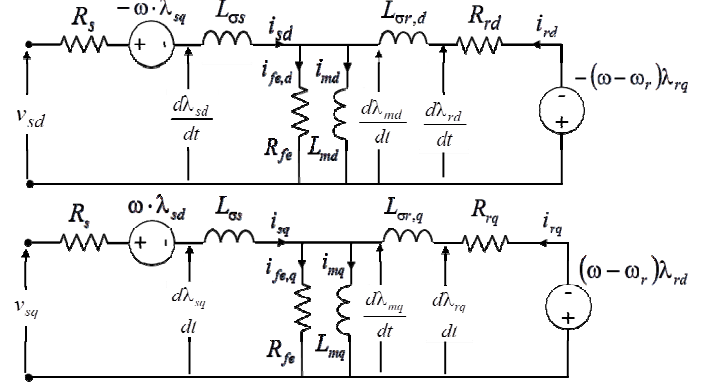


Figure 3. Dynamic equivalent circuit of LSSyR machine, in  $dq$  components.

Moreover, the magnetizing inductances are a function of both the magnetizing current components, due to saturation and cross-saturation, as usual for SyR machines. The non linear relationship is expressed in tables, relating the magnetizing flux components to the respective current components, as reported in Fig. 4. The tables are obtained by mapping the machine with static FEA.

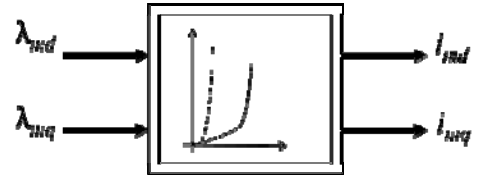


Figure 4. Non linear relationship between the magnetizing flux and current components, in the rotor reference frame  $dq$ .

The electromagnetic torque and the mechanical equation are:

$$T_{em} = \frac{3}{2} p \cdot (\bar{\lambda}_s \wedge \bar{i}_s) \quad (8)$$

$$J_{tot} \frac{d\omega}{dt} = T_{em} - T_{load} \quad (9)$$

Where  $J_{tot}$  accounts for the motor and load inertia and  $T_{load}$  is the load torque.

### B. Steady state torque as a function of the slip speed

As reported in [1] the average and pulsating torque components during run up can be described via a quasi steady

state analysis. The first assumption is that the electric and magnetic phenomena are faster than the mechanical transients, so that the slip speed can be assumed constant time by time, while the voltage vector steadily rotates around the rotor at slips speed. The steady state electrical condition corresponds to replace the time derivatives  $d/dt$  in (2)-(4) with the operator  $j(s\omega)$ , valid for steady state sinusoidal variables, as they were all phasors. The angular frequency of the phasors is  $s\omega$  because of the chosen rotor frame. The electrical equations (2)-(3) become (10) and (11) respectively:

$$\begin{cases} V_{sd} = R_s I_d + js\omega \Lambda_{sd} - \omega_r \Lambda_{sq} \\ V_{sq} = R_s I_q + js\omega \Lambda_{sq} + \omega_r \Lambda_{sd} \end{cases} \quad (10)$$

$$\begin{cases} 0 = R_r I_{rd} + js\omega \Lambda_{rd} \\ 0 = R_r I_{rq} + js\omega \Lambda_{rq} \end{cases} \quad (11)$$

Where capital letters indicate phasors. The torque expression (8) requires the stator current and flux linkage components to be expressed as  $dq$  phasors and then the vector cross-product to be calculated. To eliminate the rotor current from equations, this can be expressed as a function of the stator current by manipulation of (10) with (6) and (7).

$$\begin{cases} I_{rd} = -\frac{js\omega \cdot L_{md}}{R_{rd} + js\omega L_{rd}} I_{sd} \\ I_{rq} = -\frac{js\omega \cdot L_{mq}}{R_{rq} + js\omega L_{rq}} I_{sq} \end{cases} \quad (12)$$

Where  $L_{rd} = L_{\sigma r} + L_{md}$ ,  $L_{rq} = L_{\sigma r} + L_{mq}$ . The rotor current (12) is eliminated from equation (5) and the stator flux to current phasor relationship is found.

$$\begin{cases} \bar{\Lambda}_{sd} = \left( L_{sd} - \frac{js\omega L_{md}^2}{R_{rd} + js\omega L_{rd}} \right) \cdot \bar{I}_{sd} = \bar{Z}_{pd} \cdot \bar{I}_{sd} \\ \bar{\Lambda}_{sq} = \left( L_{sq} - \frac{js\omega L_{mq}^2}{R_{rq} + js\omega L_{rq}} \right) \cdot \bar{I}_{sq} = \bar{Z}_{pq} \cdot \bar{I}_{sq} \end{cases} \quad (13)$$

As for the rotor, also for the stator  $L_{sd} = L_{\sigma s} + L_{md}$ ,  $L_{sq} = L_{\sigma s} + L_{mq}$ . The two impedances  $Z_{pd}$  and  $Z_{pq}$  in (13) are called operational impedances: they are complex numbers intended as phasor operators, and their values are a function of the slip frequency  $s\omega$  or, in other words, of the actual rotor speed. Yet, the stator current phasors have to be calculated. The voltage to current relationship is obtained by manipulation of (10) and (13).

$$\begin{bmatrix} \bar{V}_{sd} \\ \bar{V}_{sq} \end{bmatrix} = \begin{bmatrix} (R_s + js\omega \bar{Z}_{pd}) & -(1-s)\omega \bar{Z}_{pq} \\ (1-s)\omega \bar{Z}_{pd} & (R_s + js\omega \bar{Z}_{pq}) \end{bmatrix} \cdot \begin{bmatrix} \bar{I}_{sd} \\ \bar{I}_{sq} \end{bmatrix} \quad (14)$$

The voltage  $dq$  phasors are:

$$\begin{cases} V_{sd} = -\hat{V} \cdot \sin(s\omega t + \delta_0) \\ V_{sq} = \hat{V} \cdot \cos(s\omega t + \delta_0) \end{cases} \quad (15)$$

Being the voltage phase angle  $\delta$  referenced to the  $q$  axis of the rotor, as reported in Fig. 2. When the slip speed is not zero, the  $d$  and  $q$  components of the voltage vector are then phasors in time quadrature, regardless of the term  $\delta_0$ , that is the load angle at synchronous speed:

$$\begin{cases} V_{sd} = j\hat{V} \\ V_{sq} = \hat{V} \end{cases} \quad (16)$$

The inverse of (14), finally, expresses the stator current phasors:

$$\begin{bmatrix} \bar{I}_{sd} \\ \bar{I}_{sq} \end{bmatrix} = \frac{1}{D_c} \cdot \begin{bmatrix} (R_s + js\omega \bar{Z}_{pq}) & (1-s)\omega \bar{Z}_{pq} \\ -(1-s)\omega \bar{Z}_{pd} & (R_s + js\omega \bar{Z}_{pd}) \end{bmatrix} \cdot \begin{bmatrix} j\hat{V} \\ \hat{V} \end{bmatrix} \quad (17)$$

where

$$D_c = R_s^2 + js\omega R_s (\bar{Z}_{pd} + \bar{Z}_{pq}) + (1-2s)\omega^2 \bar{Z}_{pd} \bar{Z}_{pq} \quad (18)$$

By substitution of (17) into (13), also the stator flux components are determined. The amplitude and phase of all the phasors is a function of the slip angular frequency  $s\omega$ . In Cartesian form, they are then:

$$\begin{cases} I_{sd} = a + jb \\ I_{sq} = c + jd \\ \Lambda_{sd} = e + jf \\ \Lambda_{sq} = g + jh \end{cases} \quad (19)$$

Recalling once more the torque expression (8), and substituting (13), (17) and (19), after a cumbersome manipulation, the quasi steady state torque is:

$$T_e = T_{cage} + T_{rel} \cdot \cos(2 \cdot s\omega \cdot t - \alpha) \quad (20)$$

where

$$T_{cage} = \frac{3}{2} p \cdot \left[ \frac{ce + df - ga - bh}{2} \right] \quad (21)$$

$$T_{rel} = \frac{3}{4} p \cdot \sqrt{(ce + bh - df - ga)^2 + (ed + cf - gb - ah)^2} \quad (22)$$

$$\alpha = \arctan \left( \frac{(gb + ah - ed - cf)}{(ce + bh - df - ga)} \right) \quad (23)$$

$T_{cage}$  comes from the rotor cage currents, it is constant at a given slip speed, and its value depends on the rotor slip, as in a induction motor.  $T_{rel}$  is the amplitude of the torque component produced by the rotor saliency, that is alternative and pulsating

at two times the slip angular frequency.  $\alpha$  is the phase angle of the pulsating torque component.

### C. Discussion of the two torque components

When dealing with the start-up transient of the LSSyR motor, all of a sudden switched to the AC mains, the asynchronous cage torque acts as **pull-up torque**, meaning that it is the one accelerating the motor from standstill towards synchronism. The quasi steady-state characteristic of this torque component, as a function of the rotor speed, resembles the torque characteristic of a voltage supplied IM, as represented in Fig. 5.

The reluctance torque is an alternating component at all speeds but synchronism, pulsating at twice the slip frequency during the starting phase of the motor. The steady-state envelope of  $T_{cage}-T_{rel}$  to  $T_{cage}+T_{rel}$  is represented in Fig. 5. Also the peak value  $T_{rel}$  is a function of the slip speed, as the height of the band around  $T_{cage}$  is not the same at all speeds. In particular,  $T_{cage}+T_{rel}$  at synchronous speed coincides with the **pull-out torque** of the machine: as usual for synchronous machines this is the maximum load torque that is applicable without loss of synchronism. The pull-out torque is normally much higher than the rated torque of the motor. However, having a high pull-out torque over rated torque ratio is an important figure of merit because it indicates that the motor has a high power factor at synchronous speed.

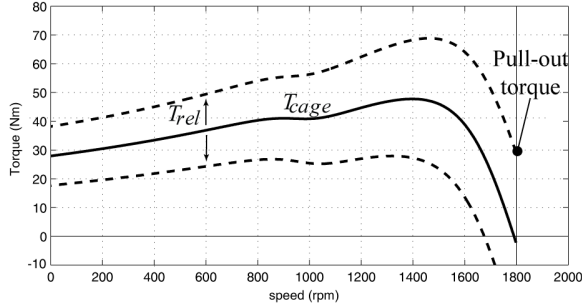


Figure 5. Quasi steady state characteristic of  $T_{cage}$  and of the  $T_{rel}$  envelope for a LSSyR motor

### D. Results from the transient and steady-state models

When line-starting a speed-dependant load such as a pump, the torque-speed transient is of the kind of the one in Fig. 6. after the initial electrical transient is extinguished, the instantaneous torque is fairly bounded within the steady state envelope. Fig. 7 shows the torque and speed transient of Fig. 6 as a function of time.

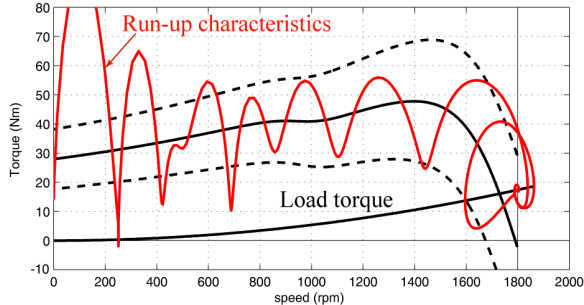


Figure 6. Start-up transient, with a load torque quadratic with speed.

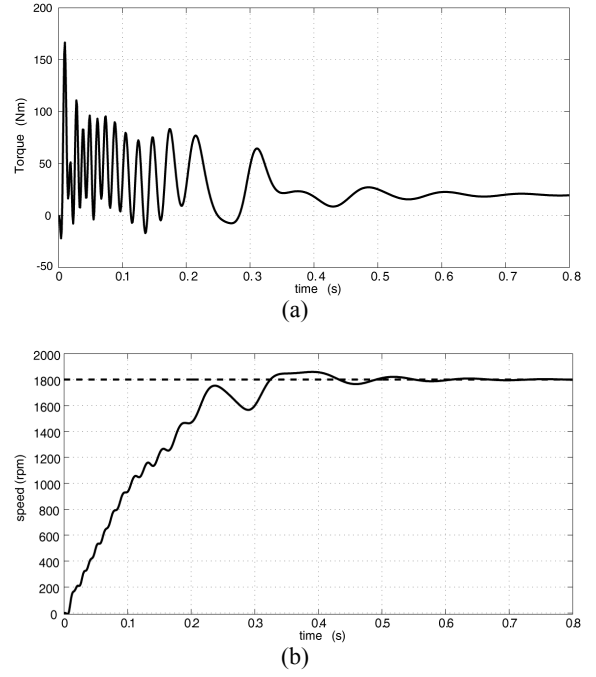


Figure 7. Torque (a) and speed (b) transients. Same simulation as Fig. 6.

### E. Pull-in torque characteristic

The **pull-in torque** is the maximum load torque under which the motor puts a given inertia into synchronism. It is then a measure of the synchronization capability of the motor and it varies inversely with the total system inertia, as in the characteristic reported in Fig. 8 for the LS2 motor of Fig. 1. The motor ratings are summarized in Table I.

For each value of inertia, the points in Fig. 8 are evaluated by repeating the transient simulations for different load levels, where the load on the Nm abscissa is intended as the load torque at synchronous speed, assuming that the load at non synchronous speed is proportional to the square of the actual rotor speed. Two curves in Fig. 8 refer to the lumped parameters model and one to the transient FEA analysis. The latter shows the best results, while the former ones show the imprecision of the lumped parameters model, and the sensitivity to the correct determination of the rotor parameters. One curve refers to the rotor parameters at zero speed, the other one close to synchronism, with the method in [8], and both cases are far from being accurate.

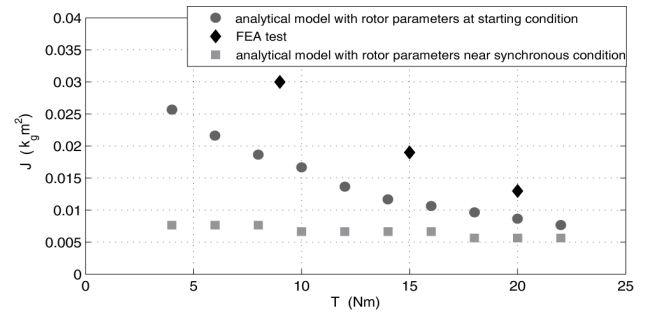


Figure 8. Pull-in torque characteristic as a function of the total inertia, for the motor LS2 of Fig. 1..

### III. DESIGN CRITERIA AND EXAMPLES

#### A. Maximization of the pull-in capability

The aim of a LSSyR design is twofold: to have a high efficiency and power factor at synchronism and also to have a pull-in torque close to the rated torque over a wide range of values inertias to be pulled-into step. The pull-in characteristics of Fig. 8 have been obtained according to the lumped parameters model presented ad section II. The imprecision demonstrated by the analytical model in Fig. 8 is related to the fact that some key aspects such as magnetic saturation and skin effect in the rotor bars are neglected, and also that the determination of key parameters such as the rotor resistances and leakage inductances is not trivial and prone to errors [8]. Yet, the model can be useful for orienteering the design, as summarized by the following considerations:

1. The performance at synchronous speed (efficiency, power factor, pull-out torque) is dominated by the saliency ratio, and saliency maximization is the correct direction to go.
2. Reducing the  $d$  and  $q$  rotor resistances improves the pull-in torque.

The example of Fig. 9 shows that halving the  $q$  rotor resistance of an example motor produces a better pull-up torque, meaning a steeper characteristic around synchronous speed and a higher value of the maximum torque at the same time. This turns to be advantageous in terms of pull-in capability, meaning that the inertia that can be pulled into step will be higher, once the rotor resistance has been reduced. As for the torque characteristic of an IM, the flip side of reducing the rotor resistance is the decrease of the stall torque, but this is only partially a problem because the skin effect, not included in Fig. 9, tends to increase the rotor resistance at high slip values, including stall, helping the stall torque to stay high. In other words, the cage torque at stall is by far underestimated in Fig. 9.

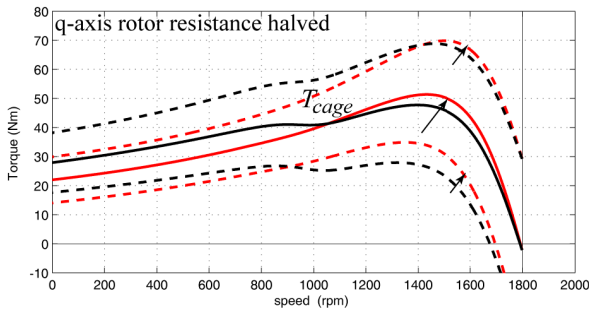


Figure 9. Effect of reducing the  $q$  axis rotor resistance on the steady-state torque characteristic of a LSSyR. Black lines refer to  $R'_{rd}=R_{rd}$ ,  $R'_{rq}=1.36R_{rq}$ .

#### B. Evolution from rotor LS1 to rotor LS3

From point (1) at subsection III.A, it turns out that SyR motors with **up to date rotors**, having a higher saliency than the ones at the time of [4], can have a better performance, at steady state, meaning a higher pull-out torque, a better power factor and then a lower torque to absorbed current ratio and then efficiency. From Fig. 9 it follows that **all available rotor**

**space must be filled with aluminum**, to have the rotor resistances as low as possible. This is also consistent with the literature, where the primordial LSSyR motors had IM-like slotted cages with limited cross section, then abandoned in favor of solutions with larger flux barriers and all the saliencies filled with aluminum [6], such as the Synduction motor in [4].

The starting point of the design evolution described by the three rotors in Fig. 1 All three motors have the same stator, taken from a 2.2 kW, four pole, 50 Hz IM competitor, whose drawings are not reported. The LS1 design is the like of a Synduction motor, designed according to [4] to comply with the common stator. The rotor LS2 is a state of the art SyR rotor designed for vector control. The LS3 one is the final LSSyR solution proposed here, with a much increased pull-in capability.

#### C. Improvement of the pull-in capability

The pull-into step characteristics of the three LSSyR motor examples are reported in Fig. 10. The pull-in torque versus the total inertia is reported for the three machines.

The maximum inertia pulled-in by the LS1 motor at nominal torque (14.2 Nm) is  $0.020 \text{ kg m}^2$  (four times the inertia of the motor). At lower loads, the feasible inertia is larger.

The state of the art SyR rotor LS2, having four layers, is designed with the criteria in [7] and then filled with aluminum. Its pull-in capability is close to the one of the Synduction-like motor LS1, at rated load. It is less variable with inertia, with respect to LS1, and then lower at lower inertias and vice-versa at higher inertias.

Last, the proposed LS3 geometry has a pull-in capability improved by 50% with respect to LS2 at all values of inertia. With respect to LS2, the cross section of the four saliencies is increased as much as possible and, most of all, the steel layer on top of the  $q$  axis has been removed for making room to more aluminum and reduce the  $d$  and  $q$  rotor resistances.

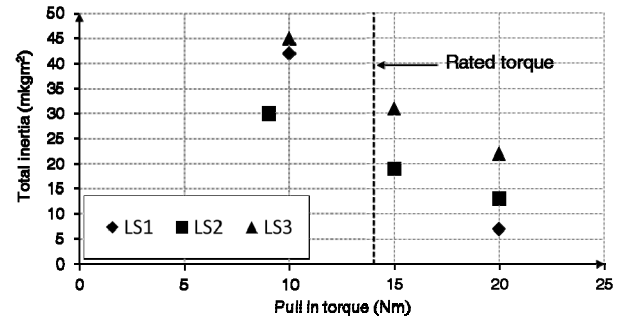


Figure 10. Pull-in torque characteristics of motors LS1 to LS3, evaluated with transient FEA.

#### D. Comparison of the steady-state performance

Table I reports the steady state performance of the three LSSyR examples, at rated load. The table includes also the performance of the benchmark IM, for the quantification of the improvements in efficiency. All the results come from FEA. The stator copper and rotor aluminum temperatures are

assumed to be 120 C, although the four motors have slightly different losses.

The steady state performance of the LS1 motor is comparable to the one of the IM, meaning that the efficiency is a little higher and the power factor is lower, resulting in a higher stator current (5.8 A versus 5.0 A).

For what concerns LS2, the steady state efficiency grows significantly with respect to S1, as it can be expected due to the much higher saliency and then torque to Ampere ratio at synchronism. The final solution LS3 has a little decrease in performance at steady-state, because it is no longer designed exactly for synchronous operation, but still maintains a good efficiency while increasing the pull-in capability significantly.

TABLE 1: STEADY STATE PERFORMANCE OF THE EXAMPLE MACHINES AT NOMINAL LOAD

|                     |            | LS1   | LS2   | LS3          | Induction motor |
|---------------------|------------|-------|-------|--------------|-----------------|
| Line Voltage        | [V]<br>rms | 398   | 398   | 398          | 398             |
| Phase Current       | [A]<br>rms | 5,8   | 4,79  | 4,95         | 5,0             |
| Continuous Torque   | [Nm]       | 14,2  | 14,2  | 14,2         | 15,1            |
| Rated Speed         | [rpm]      | 1500  | 1500  | 1500         | 1381            |
| Output Power        | [W]        | 2231  | 2231  | 2231         | 2183            |
| Rated Power Factor  |            | 0,718 | 0,763 | 0,745        | 0,794           |
| Core loss           | [W]        | 61    | 48    | 50           | 50              |
| Joules loss, stator | [W]        | 439   | 299   | 318          | 330             |
| Joule loss, rotor   | [W]        | 121   | 31    | 48           | 168             |
| Windage loss        | [W]        | 31    | 31    | 31           | 31              |
| Efficiency          |            | 0,773 | 0,845 | <b>0,834</b> | <b>0,790</b>    |

#### IV. EXPERIMENTAL RESULTS

To validate the conclusion at section III, the results of the transient FEA are experimentally validated on a LSSyR motor prototype, whose rotor drawing is reported in Fig.11. This motor, originally equipped with permanent magnets (PM) and intended for traction, is the one used in [9], whose main ratings are reported in Table II.

TABLE 2I: RATINGS OF THE PM-ASSISTED PROTOTYPE MOTOR PRIOR TO BE MODIFIED FOR THE EXPERIMENTS AS LSSyR

|                  |     |       |
|------------------|-----|-------|
| Continuous Power | kW  | 7     |
| Peak Power       | kW  | 10    |
| Base speed       | rpm | 2450  |
| Max speed        | rpm | 10000 |
| Rated Current    | A   | 20    |
| Rated Voltage    | V   | 257   |

Here the PMs have been removed from the rotor and

copper bars have been inserted instead into the saliencies, and then welded at the hands to copper end rings. Fig. 11 shows the cross section of the rotor laminations and the areas where the copper has been inserted. The tests have been divided into two stages. At first, the cage is only in the three bigger layers of each pole, as represented by the grey copper bars in Fig. 11. Later on, the red copper bars have been added into the fourth layer, the smallest one. Fig. 12 reports the picture of the rotor prototype, in versions 1 and 2, before and after the insertion of the small red bars.

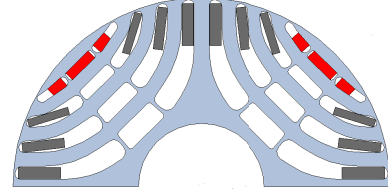


Figure 11. Rotor lamination of the PM-assisted SyR of [9], modified to house a copper cage. Version 1 has only the copper bars in grey, version 2 has also the red bars in the outer layers.

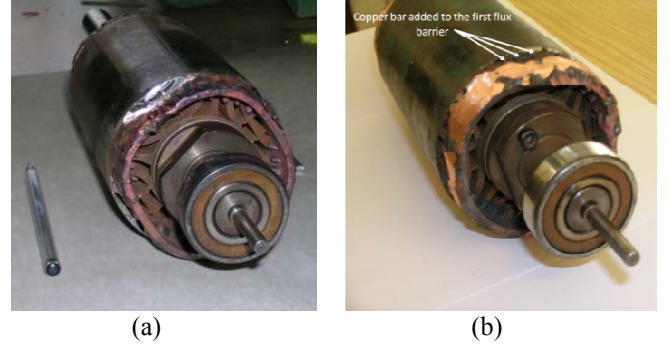


Figure 12. Rotor used for the experimental tests. a) Version 1; b) Version 2

#### A. Experimental setup

Fig. 13 exhibits the equipment used for the tests. The inertia of the LSSyR prototype has been measured by accelerating the rotor by means of a known force applied with a known lever. The inertia of Version 1 is  $J_{mot} = 0.0057 \text{ kgm}^2$ . Version 2 has been assumed to have the same inertia, which is wrong but of little impact when more rotating bodies other than the motor are involved.



Figure 13. LSSyR motor prototype loaded by the DC machine.

The load torque is produced by a DC servomotor of the AXEM series [10]. Its inertia is  $0.0067 \text{ kgm}^2$ . The total inertia of LSSyR prototype, DC machine and coupling is  $J_{tot} = 0.0124 \text{ kgm}^2$  (2,2 times the one of motor alone). The inertia can be increased by including a disk of steel between the two motors, leading to a total inertia of  $0.021 \text{ kgm}^2$ . The DC machine is loaded with a resistor, producing a torque that is proportional to the speed. The resistance can be varied to change the load torque curve. The LSSyR prototype is line started at 153V, 50Hz, compatible with the specifications of Table II, that refer to a machine designed for being inverter driven.

### B. Pull-in capability of Versions 1 and 2

The pull-in characteristic of the LSSyR prototype, FEA evaluated, is reported in Fig. 14. The best experimental start-ups are also reported, for the two versions. The experimental tests refer to only two values of inertia, that are with and without the additional disk for extra inertia. The load torque has been varied progressively until the motor is no longer capable of synchronization. The difficulty of running comprehensive tests stands in the effect of temperature. At cold conditions the pull-in torque is the one reported in Fig. 14. After a couple of successful start beginning from cold, however, the rotor temperature is no longer the same, and the pull-in capability is reduced. If, for instance, one wants to repeat the same test many times for taking into account the effect of voltage phase at time zero, this is not possible because every time the temperature has changed. It is then necessary to wait until the machine (the rotor, in particular) is at room temperature again before running a new test.

From the data related to Version 2, a good agreement is found at the highest value of inertia, that gives a pull-in torque around the rated torque value. At lower inertia the pull-in torque is much lower than the FEA evaluated one, but still we have some doubt about how comprehensive the test campaign has been.

The comparison between Versions 1 and 2 confirms the beneficial effect of the extra rotor bars. The pull-in torque is more than doubled.

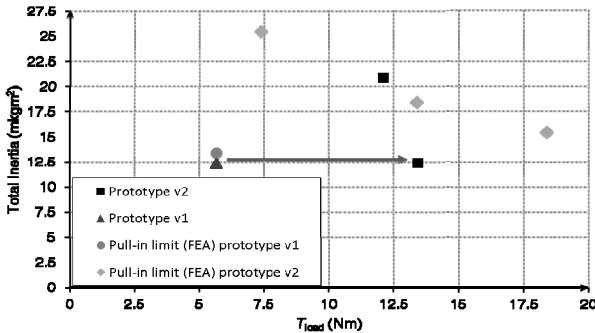


Figure 14. Pull-in characteristic of the prototype motor, in Versions 1 and 2, calculated with FEA and measured.

### C. Speed transients

The experimental and the FEA speed transients at start-up are reported in Fig. 15 for Version 1 and in Fig. 16 for Version

2.

Fig. 15 shows a good agreement between FEA and measures, and puts in evidence the effect of the initial phase of the voltage vector. The load torque and total inertia are the ones reported in the characteristic of Fig. 14 (triangle marker).

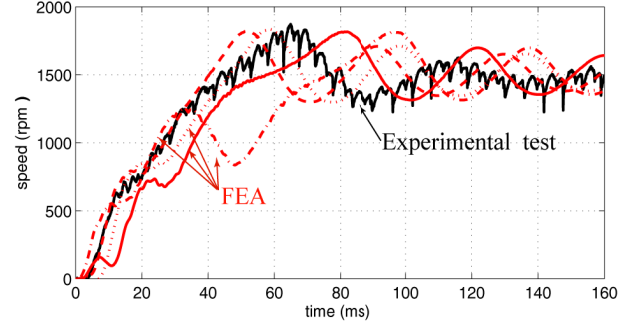


Figure 15. Line start speed transient with Version 1 rotor. Total inertia is  $12.4 \cdot 10^{-3} \text{ kgm}^2$  and  $T_{load}$  is 5.66 Nm. Black line: measured. Red lines: FEA calculated with different initial voltage phase values.

In Fig. 16 the two tests indicated with square markers in Fig. 14 are reported. In Fig. 16b, the one at high inertia, it is possible to see that the actual start transient converges at first to a sub synchronous speed and completes the synchronization in a second time. This never occurs with FEA.

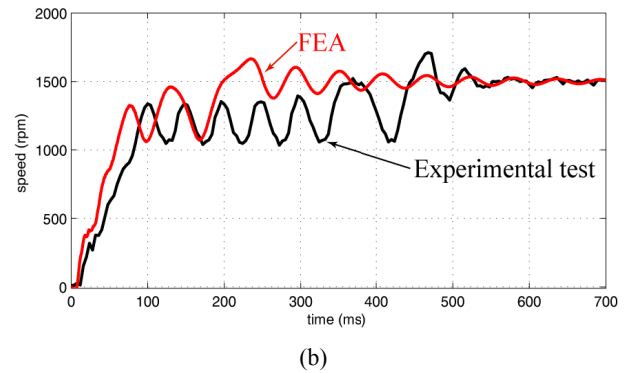
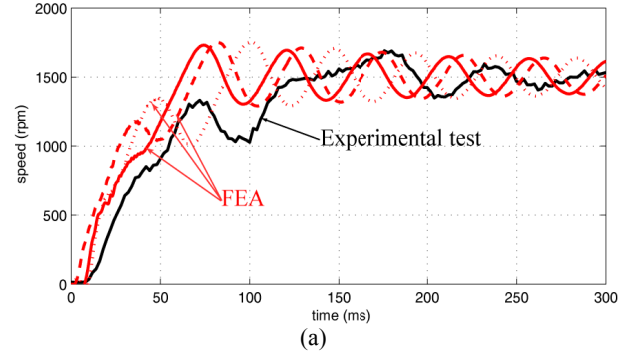


Figure 16. Line start speed transient with Version 2 rotor. Total inertia is  $12.4 \cdot 10^{-3} \text{ kgm}^2$  (a) and  $20.9 \cdot 10^{-3} \text{ kgm}^2$  (b).  $T_{load}$  is 13.4 Nm (a) and 12.0 Nm (b). Black line: measured. Red lines: FEA calculated.

## V. CONCLUSION

The design and the performance of Line-Start, Synchronous Reluctance motors have been modeled and experimentally

verified. State of the art-SyR rotors show a better performance of LSSyR motors in the literature, and show to be competitive towards induction motor counterparts in terms of efficiency. The effect of filling as much space as possible with rotor conductors has been put in evidence, both in the model and experimentally. Future works will deal with the evaluation of the further optimization of the motor starting capability, by means of the choice of the number of layers and their placement.

#### REFERENCES

- [1] Honsinger, V.B.; , "Permanent Magnet Machines: Asynchronous Operation," *Power Apparatus and Systems, IEEE Transactions on*, vol.PAS-99, no.4, pp.1503-1509, July 1980.
- [2] Miller, T. J. E.; , "Synchronization of Line-Start Permanent-Magnet AC Motors," *Power Engineering Review, IEEE*, vol.PER-4, no.7, pp.57-58, July 1984
- [3] Kurihara, K.; Rahman, M.A.; , "High-efficiency line-start interior permanent-magnet synchronous motors," *Industry Applications, IEEE Transactions on*, vol.40, no.3, pp. 789- 796, May-June 2004.
- [4] VB Honsinger; "Synchronous Reluctance Motor", US Patent 3,652,885, March 1972
- [5] Lawrenson, P.J.; Mathur, R.M.; , "Pull-in criterion for reluctance motors," *Electrical Engineers, Proceedings of the Institution of*, vol.120, no.9, pp.982-986, September 1973
- [6] Pettit, R.; Wagner, P.; Shaw, K.; , "Synchronous AC motors for process control over wide speed ranges ," Textile Industry Technical Conference, 1988., IEEE 1988 Annual , vol., no., pp.6/1-6/8, 4-5 May 1988
- [7] Vagati, A.; Franceschini, G.; Marongiu, I.; Troglia, G.P.; , "Design criteria of high performance synchronous reluctance motors ," *Industry Applications Society Annual Meeting, 1992., Conference Record of the 1992 IEEE*, vol., no., pp.66-73 vol.1, 4-9 Oct 1992.
- [8] Boroujeni, S.T.; Bianchi, N.; Alberti, L.; , "Fast Estimation of Line-Start Reluctance Machine Parameters by Finite Element Analysis," *Energy Conversion, IEEE Transactions on* , vol.26, no.1, pp.1-8, March 2011
- [9] Pellegrino, G.; Armando, E.; Guglielmi, P., "Direct Flux Field-Oriented Control of IPM Drives With Variable DC Link in the Field-Weakening Region," *Industry Applications, IEEE Transactions on* , vol.45, no.5, pp.1619,1627, Sept.-oct. 2009
- [10] Axem Servo Motors, <http://www.parker.com/>
- [11] Magnet 7.3.0, by Infolytica Corporation. <http://www.infolytica.com/>